

# Relativistic EOM-CCSD for core-excited and core-ionized state energies based on the 4-component Dirac-Coulomb(-Gaunt) Hamiltonian.

Loïc Halbert,<sup>1, a)</sup> Marta L. Vidal,<sup>2, b)</sup> Avijit Shee,<sup>3, c)</sup> Sonia Coriani,<sup>2, d)</sup> and André Severo Pereira Gomes<sup>1, e)</sup>

<sup>1)</sup> Université de Lille, CNRS, UMR 8523 – PhLAM – Physique des Lasers, Atomes et Molécules, F-59000 Lille, France

<sup>2)</sup> Department of Chemistry, Technical University of Denmark, DK-2800 Kongens Lyngby, Denmark

<sup>3)</sup> Department of Chemistry, University of Michigan, Ann Arbor, Michigan 48109, USA

We report an implementation of the core-valence separation approach to the 4-component relativistic Hamiltonian based equation-of-motion coupled-cluster with singles and doubles theory (CVS-EOM-CCSD), for the calculation of relativistic core-ionization potentials and core-excitation energies. With this implementation, which is capable of exploiting double group symmetry, we investigate the effects of the different CVS-EOM-CCSD variants, and the use of different Hamiltonians based on the exact 2-component (X2C) schemes, on the energies of different core ionized and excited states in halogen ( $\text{CH}_3\text{I}$ ,  $\text{HX}$  and  $\text{X}^-$ ,  $\text{X} = \text{Cl-At}$ ) and xenon containing ( $\text{Xe}$ ,  $\text{XeF}_2$ ) species. Our results demonstrate that the 2-component molecular mean-field ( $^2\text{DC}^M$ ) approach is not only capable of providing core excitations and ionization energies that are clearly superior to the atomic mean-field approximation when the Gaunt interaction is included, but also nearly indistinguishable from the reference 4-component DC energies.

## I. INTRODUCTION

X-ray spectroscopies, which typically probe core electrons through electronic excitation or ionization, are particularly suitable techniques to study the local environment of atoms, molecules and materials, as the localized nature of the core orbitals makes them very selective and sensitive.<sup>1,2</sup>

Over the last few years, new X-ray free electron lasers (XFEL) and last generation synchrotrons have started operating. These advanced light sources have opened the door to a variety of new X-ray-based spectroscopies,<sup>3–5</sup> including those operating in time-resolved and non-linear regimes.<sup>2–6</sup> As stated for instance by Milne, Penfold and Chergui in their review:<sup>7</sup> “[...] *The progress of experimental techniques for core level spectroscopies is unraveling subtle spectral features implying that high level theoretical approaches are required to interpret them* [...]”. The experimental X-ray spectra need to be compared to highly accurate theoretical calculations to assign spectral features and to relate experimental measurements to the structure and dynamic properties of the probed molecular system.

Among the methods one can use to simulate inner-shell spectra<sup>2</sup>,  $\Delta\text{SCF}$  stands out because of its decent results at a fairly low computational cost, and similar approaches can be devised using correlated approaches such as  $\text{MP2}$ <sup>8</sup> or coupled-cluster (CC).<sup>9</sup> However, methods that diagonalize the same Hamiltonian — for in-

stance, wavefunction-based approaches such as multireference configuration interaction (MRCI) and equation of motion CC (EOM-CC), or Green’s functions-based approaches such as the algebraic diagrammatic construction (ADC), or time-dependent density functional theory (TDDFT) — have the advantage of keeping a set of orthonormal electronic states, which greatly simplify the calculation of transition moments.

Among these, CC methods have the distinct advantage of accurately treating electron correlation and also of including a good deal of relaxation effects.<sup>10,11</sup> These methods have been efficiently extended to the core space by exploiting the core valence separation (CVS) approximation<sup>12</sup> in the non-relativistic domain.<sup>13–16</sup> The core-valence separation is justified by the large spatial and energetic separation between valence and core orbitals/electrons. On the one side, CVS allows to straightforwardly address the highly-energetic core states with minor modifications to preexisting eigenvalue solvers. On the other side, the CVS helps alleviating convergence issues due to the large number of valence ionized states in the frequency region of the core excitations.<sup>17,18</sup>

Relativistic effects<sup>19,20</sup> can significantly alter the energies of inner electrons, and consequently the core spectra of atoms and molecules: due to the high velocities of their electrons (a significant fraction of the speed of light), core  $s$  and  $p$  orbitals contract (with an associated lowering of their orbital energies) while, due to increased screening,  $d$  and  $f$  orbitals expand (with an associated increase in their orbital energies). At the same time, orbitals which are degenerate in a non-relativistic framework ( $p$ ,  $d$ ,  $f$ ) are strongly split due to spin-orbit coupling, and particularly so for the innermost orbitals.

Relativistic effects are so pronounced in the core region that, even for molecules containing only elements of the first and second rows, they are very important for the accurate determination of K and L edge spectra. While

<sup>a)</sup> Electronic mail: [loic.halbert@univ-lille.fr](mailto:loic.halbert@univ-lille.fr)

<sup>b)</sup> Electronic mail: [malop@kemi.dtu.dk](mailto:malop@kemi.dtu.dk)

<sup>c)</sup> Electronic mail: [ashee@umich.edu](mailto:ashee@umich.edu)

<sup>d)</sup> Electronic mail: [soco@kemi.dtu.dk](mailto:soco@kemi.dtu.dk)

<sup>e)</sup> Electronic mail: [andre.gomes@univ-lille.fr](mailto:andre.gomes@univ-lille.fr)

even rather approximate treatments of relativistic effect can yield accurate results for light elements,<sup>9,21–24</sup> a more consistent way of treating these effects is through an electronic Hamiltonian based on the 4-component Dirac operator, as it is accurate all the way down to the heaviest elements (transition metals, lanthanides and actinides). As such, 4-component based methods are ideally suited to treat the core spectra across the periodic table, and to probe K, L and M edges of heavy elements,<sup>8,25,26</sup> which are much more complex to interpret than those for lighter elements.

In this study, we present an approach to study core ionization (and excitation) through the use of projectors, inspired by the work of [Coriani and Koch](#),<sup>13</sup> but extended to the 4-component EOM-CCSD approach developed by Shee *et al.*<sup>27</sup> in the DIRAC relativistic electronic structure package.<sup>28</sup>

The paper is organized as follows: In Section II, we give a brief outline of EOM-CCSD (II A) and of CVS (II B), as well as the details of the current implementation (II C). In Section III, we provide the computational details of the calculations. In Section IV, we present the results obtained with the newly implemented method, where we discuss the accuracy of the CVS approximation (IV A), the performance of the different CVS variants (IV B), the influence of the Hamiltonian (IV C) and the comparison to experiment for ionization (IV D) and excitation (IV E) energies. Finally, Section V summarizes our conclusions.

## II. METHODS AND IMPLEMENTATION

### A. EOM-CC

In EOM-CC, the ground-state is treated at the coupled-cluster level. Its eigenfunction is hence given by the exponential ansatz:

$$|\Psi_{CC}\rangle = e^{\hat{T}}|\Phi_0\rangle; \quad \hat{T} = \sum_{\mu} t_{\mu}\hat{\tau}_{\mu} \quad (1)$$

where  $\Phi_0$  is the reference (typically Hartree-Fock) determinant and the operator  $\hat{T}$  is the cluster operator. Truncating  $\hat{T}$  to single (S) and double (D) excitations yields the coupled-cluster singles-and-doubles (CCSD) model:

$$\hat{T} = \hat{T}_1 + \hat{T}_2; \quad \hat{T}_1 = \sum_{ia} t_i^a a_a^\dagger a_i; \quad \hat{T}_2 = \frac{1}{4} \sum_{ijab} t_{ij}^{ab} a_a^\dagger a_b^\dagger a_j a_i, \quad (2)$$

The energy and the cluster amplitudes are found from the CC equations:

$$\langle \Phi_0 | \hat{H} | \Phi_0 \rangle = E \quad (3)$$

$$\langle \Phi_{\mu} | \hat{H} | \Phi_0 \rangle = 0; \quad |\Phi_{\mu}\rangle = \hat{\tau}_{\mu} |\Phi_0\rangle, \quad (4)$$

where the similarity-transformed Hamiltonian  $\hat{\bar{H}}$  has been defined as:

$$\hat{\bar{H}} \equiv e^{-\hat{T}} \hat{H} e^{\hat{T}}. \quad (5)$$

In the equation-of-motion coupled-cluster (EOM-CC) method<sup>10,29</sup> the target states are obtained by the diagonalization of the non-Hermitian similarity-transformed Hamiltonian. This non-Hermiticity gives rise to right ( $R$ ) and left ( $L$ ) eigenvectors that are not adjoints of each other, obtained solving two different eigenvalue equations:

$$\hat{\bar{H}} |R_{\mu}\rangle = E_{\mu} |R_{\mu}\rangle \quad (6)$$

$$\langle L_{\mu} | \hat{\bar{H}} = E_{\mu} \langle L_{\mu} |, \quad (7)$$

for a given excited state  $\mu$  with energy  $E_{\mu}$ , where the eigenstates are chosen to satisfy the biorthogonality condition:

$$\langle L_{\mu} | R_{\nu} \rangle = \delta_{\mu\nu}. \quad (8)$$

Right and left wavefunctions of the target states have been thus obtained from a linear parametrization of the reference state through the  $\hat{R}$  or  $\hat{L}$  operators

$$|\Psi_{\mu}\rangle = e^{\hat{T}} \hat{R}_{\mu} |\Phi_0\rangle \quad (9)$$

and

$$\langle \bar{\Psi}_{\mu} | = \langle \Phi_0 | \hat{L}_{\mu} e^{-\hat{T}}. \quad (10)$$

Therefore, the choice of the  $\hat{R}$  and  $\hat{L}$  operators defines which target states to study, yielding different EOM-CC models. In the present work we focus on the models for electronically excited (EE) states and ionization potentials (IP):

- EOM-CCSD-EE:

$$\hat{R}^{\text{EE}} = r_0 + \sum_{ia} r_i^a \{a_a^\dagger a_i\} + \sum_{i>j, a>b} r_{ij}^{ab} \{a_a^\dagger a_b^\dagger a_j a_i\} \quad (11)$$

$$\hat{L}^{\text{EE}} = l_0 + \sum_{ia} l_i^i \{a_i^\dagger a_a\} + \sum_{i>j, a>b} l_{ab}^{ij} \{a_i^\dagger a_j^\dagger a_b a_a\} \quad (12)$$

- EOM-CCSD-IP:

$$\hat{R}^{\text{IP}} = \sum_i r_i \{a_i\} + \sum_{i>j, a} r_{ij}^a \{a_a^\dagger a_j a_i\} \quad (13)$$

$$\hat{L}^{\text{IP}} = \sum_i l_i^i \{a_i^\dagger\} + \sum_{i>j, a} l_{ij}^a \{a_j^\dagger a_i^\dagger a_a\} \quad (14)$$

where curly brackets refer to normal ordering with respect to the Fermi vacuum defined by the reference  $\Phi_0$ , and the sets  $\{\mathbf{r}\}$ ,  $\{\mathbf{l}\}$  to the amplitudes of the corresponding operators.

We have here truncated our  $\hat{R}$  and  $\hat{L}$  operators at the singles-doubles level since the same truncation is used for the  $\hat{T}$  operators.

## B. The core-valence separation approximation

The essence of the core-valence separation (CVS) approximation<sup>12</sup> is to decouple valence and core electrons based on their difference in energy and spatial extension. This allows to solve the regular, in this case, EOM-CC equations only in the space of the relevant orbitals. However, different flavours of CVS exist, which introduce different levels of approximation. Coriani and Koch first introduced the CVS approximation within coupled-cluster theory<sup>13,14</sup> by applying a projector that zeroes out the amplitudes of all excitations that do not involve at least one core electron. Recently, the frozen-core (fc) CVS-EOM-CCSD approach has been proposed that introduces a further approximation, in this case at the ground-state level: the core orbitals are frozen when solving the CC equations for the ground-state whereas they are the only active ones when solving the EOM equations. Both schemes retain the contribution from excitations simultaneously involving two core orbitals. However, these excitations are located in a much higher range of energy in the spectrum and might therefore also be decoupled. This is the strategy adopted for instance by Dreuw and co-workers in their implementation of the CVS within the ADC family of methods.<sup>30</sup>

In this work, the CVS implementation has been carried out following the recipe proposed by Coriani and Koch:<sup>13</sup> a projector  $P$  is applied at each iteration of the Davidson procedure during the resolution of the EOM-CC equations. This projector  $P$  selectively zeroes out the unwanted contributions to the EOM trial/solution vectors according to the approximation used. In the CVS approach, unwanted contributions generally correspond to excited determinants involving only occupied valence ( $v$ ) spinors. In the case of EOM-EE, the application of a projector  $P \equiv P^{\text{CVS}}$  to a target electronic state  $|\Psi_\mu^{\text{EE}}\rangle$  corresponds to

$$P^{\text{CVS}}|\Psi_\mu^{\text{EE}}\rangle \implies \mu r_i^a = \mu r_{ij}^{ab} = 0 \text{ if } i, j \in v, \quad (15)$$

though one can also devise variants in which additional contributions are zeroed out, see Section II C for details. With this definition, the eigenvalue equation to be solved in order to get the energy of the target states becomes:

$$P^{\text{CVS}} \left( \hat{H} P^{\text{CVS}} |R_\mu\rangle \right) = E_\mu P^{\text{CVS}} |R_\mu\rangle \quad (16)$$

It should be noted that the projection scheme does not yield any savings, in terms of memory usage or operations. Some of us<sup>15</sup> have recently gone beyond the use of projection operators and introduced an analytical formulation of CVS, in which only the sub-blocks of the similarity-transformed Hamiltonian that are relevant to the calculation of a given core level are actually formed, thus resulting in a more efficient implementation. This formulation is naturally combined with the frozen-core approximation separating valence and core spaces. However, one may argue it introduces at the same time an additional error from neglecting core correlation.<sup>15</sup>

## C. Implementation details

In this work we focus on exploring the definition of different CVS variants and on assessing their performance following the projection-based scheme, due to its ease of implementation, and with it in view of later implementing the analytical formulation in DIRAC.

We have based our implementation on a flexible scheme to define projection operators.

- (a) A mapping is defined between the excited determinants (and the virtual and occupied spinors' energies associated with each) and the position of each excited determinant in the storage of the ground-state CC amplitudes and EOM-CC coefficients (in the RELCC module of DIRAC these are stored in triangular form, and blocked by symmetry, for details see 31–33);
- (b) Information is gathered on how the excited determinant space  $\{v\}$  will be treated, i.e. whether retained ( $P^v = 1$ ) or projected out ( $P^v = 0$ ). We have made two options available to the user, based on spinor energies: (i) restricted excitation windows (REWs) for the occupied and virtual. This is achieved by setting a lower and an upper bound for the spinor's energies; and (ii) CVS, via a single energy that acts as the threshold for the separation between core and valence.
- (c) Using the information from the previous steps, suitable one-particle (singly ionized or excited) unit trial vectors for the core states are then generated, using the values of the diagonal of  $\bar{H}$  within the subspaces defined in (b).

It is important to note that in our implementation, tracking the core excited or ionized states requires the use of a root homing procedure, in which new trial vectors are created by maximizing their overlap with the preceding ones.

In addition to CVS and REW for the excited states, we also used the projection setup to implement the frozen-core approximation, such that we can project out the amplitudes corresponding to core ( $c$ ) orbitals at each iteration during the resolution of the ground-state amplitude equations:

$$P^{\text{core}}|\Psi_{\text{CC}}\rangle \implies t_i^a = t_{ij}^{ab} = 0 \text{ if } i, j \notin v \quad (17)$$

## III. COMPUTATIONAL DETAILS

All coupled-cluster calculations were carried out with the DIRAC19<sup>34</sup> version of the DIRAC electronic structure code,<sup>28</sup> employing Dyall's basis sets<sup>35–38</sup> of triple-zeta quality (dyall.acv3z)<sup>39</sup> for all species. For selected calculations, on heavy atoms only, we performed extrapolations to the complete basis set limit by considering, in

addition, quadruple-zeta quality Dyall (dyall.acv4z) basis sets. Unless otherwise noted, all occupied and virtual spinors were considered in the correlation treatment.

We employed the Dirac–Coulomb (DC) Hamiltonian as well as its molecular mean-field<sup>40</sup> approximations ( ${}^2\text{DC}^M$ ), and the molecular mean-field approximation to the Dirac–Coulomb–Gaunt Hamiltonian ( ${}^2\text{DCG}^M$ ), where the Gaunt-type integrals are explicitly taken into account only during the SCF step, due to the fact that the transformation of these to MO basis is currently not implemented. In addition to these, we performed X2C calculations employing the atomic mean-field approximation.

Unless otherwise noted, we employed the usual approximation of the energy contribution from ( $SS|SS$ )-type two-electron integrals by a point-charge model.<sup>41</sup> As it will be discussed below, this approximation introduces negligible errors ( $< 0.01$  eV) for lower-energy edges. However, for the higher-energy edges of the heavier systems, its error becomes important.

The  $\text{XeF}_2$  structure was taken from Ref. 42. It corresponds to an optimised structure obtained at the SFX2C-1e/coupled-cluster single double triple (CCSD(T))/unc-atomic natural orbital (ANO)-RCC level ( $r_{\text{Xe-F}} = 1.9736$  Å). The coordinates of  $\text{CH}_3\text{I}$  come from experimental data in Ref. 43. Finally, the coordinates for  $\text{HX}$  were taken from Ref. 44.

The dataset can be retrieved at the Zenodo repository.<sup>45</sup>

### A. Approximations used in CVS

Beside the original CC-CVS approach,<sup>13</sup> we have in addition investigated other approximations:

1. Further restricting the definition of the projectors to also drop excited configurations with two core indices (ND, for “No Doubly occupied core”)
2. Freezing the core in the ground-state calculation, retaining thus only the valence orbitals, typically defined as the orbitals with the highest principal quantum number  $n$ , for each possible value of azimuthal quantum number  $l$  (FC-V).
3. Freezing all core orbitals except those that are to be targeted in the EOM step (FC-V-except).
4. The definition of the core/valence spaces follows that of the CVS definition/threshold, that is, only the core orbitals with same or lower energy than the ones belonging to the edge under investigation are frozen (FC-f).
5. Further restricting the number of frozen core spinors to only those below the ones of the edge of interest (FC-fpMO *frozen core - follow previous MO*)

The variants ND and FC-V were also employed with REWs. Since the performance of REW variants was always found to be inferior to their CVS equivalents, they will not be discussed here. The results are however available as supplemental information.

## IV. RESULTS

As outlined above, apart from the different Hamiltonians at our disposal, the original CVS formulation itself can be modified through a number of different approximations. In order to draw a clearer picture of their interactions, we proceed in a stepwise fashion:

First, using the  ${}^2\text{DC}^M$  Hamiltonian and focusing on core ionizations, we compare (A) the performance of CVS-EOM-CCSD to the original EOM-CCSD; and (B) the impact of the different approximations that can be introduced in the CVS method itself (see Section III A).

Then, having established the relative accuracy of CVS, we investigate (C) the effect of the Hamiltonians on the core ionization energies, and finally (D) proceed to a comparison to experiment of the most accurate setup, focusing mostly on core ionization but also discussing selected core excitations (E).

In what follows we will not discuss basis set effects. Nonetheless, in Figure 1, we show for  $\text{I}^-$  a typical behavior: first, there is very little difference between triple and quadruple zeta results (with differences between 0.05 and 0.2 eV), making the corrections due to basis set incompleteness so small that we consider these to be unnecessary. Second, if there are non-negligible differences between the convergence of  $s$ ,  $p$  and  $d$  shells as the basis sets are improved, the double-zeta basis sets also yield results which are quite good, with differences in binding energies with respect to the triple zeta results no larger than around 0.4 eV, a behavior that may make these smaller basis sets interesting for calculations on larger molecules.

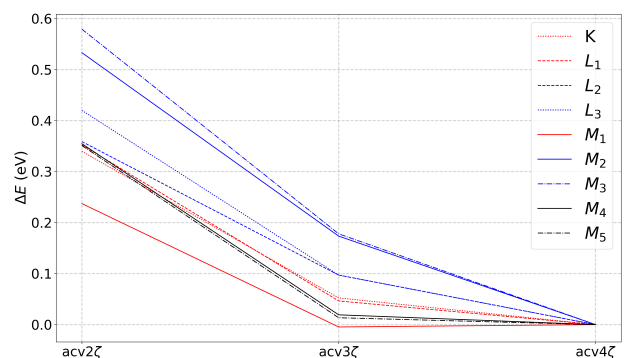


FIG. 1: Basis set influence (Dyall basis sets) on the core binding energies of  $\text{I}^-$  using the CVS approach.

These conclusions are in line with earlier basis set analyses on light elements.<sup>21,46</sup> In the basis set convergence



study by Sarangi *et al.*,<sup>46</sup> in particular, it was shown that, for systems containing only light elements, uncontracted basis sets, even of relatively modest quality for the valence, can provide quite reliable core binding energies.

### A. A comparison of CVS-EOM-IP-CCSD and EOM-IP-CCSD

As mentioned above, the CVS approach provides an efficient and robust way of targeting the low-lying core states. Quantifying the errors introduced by it is therefore an important issue, and we note proposals for methods to estimate it. Coriani and Koch<sup>13</sup> evaluated the errors of their CVS variant by comparing to full-space Lanczos results, finding deviations of at most a few hundredths of eV. The authors also proposed a perturbative correction obtained using a Löwdin partition of the Jacobian and the eigenvalue equation. A recent study by Herbst and Fransson<sup>47</sup> shows that the CVS error is small and stable across multiple systems within the algebraic diagrammatic method (ADC). Thus, we expect to find the same trend for CC. This article also reports the implementation of a post-processing step which removes the error to assess its significance.

Here, we can harness the ability of DIRAC to exploit linear symmetry, and directly compare, for selected species, the CVS-EOM-IP-CCSD states with those obtained by the full diagonalization of the different symmetry blocks of similarity-transformed Hamiltonian.

The difference between the two approaches is shown graphically for  $I^-$  in Figure 2. Due to the very dense spectra of  $\bar{H}$ , in the top half of the figure we do not display individual states but rather the number of states per 0.37 Ha intervals. Note that, for technical reasons related to the plotting library used, in this figure we present energies in Hartree, while elsewhere we employ electronvolts. We further discriminate between all states (black) and those containing contributions from singly ionized configurations contributing to at least 1% of the total wavefunction (red).

Upon having a closer look at the singly ionized states at the bottom half of the figure, we can more clearly see how the singly ionized states obtained with the CVS approximation (labelled “CVS”) closely match a subset of those obtained by the full diagonalization (labelled “full”) of  $\bar{H}$ .

We note that the additional states presented for the “full” calculation correspond to states that contain significant singly-ionized character but also small but non-zero  $2h1p$  contributions. The presence of such states hint at potential pitfalls when targeting only a subset of such highly excited states for some of the L and M edges—not so much in terms of convergence (we have not encountered particular difficulties in converging our calculations) but rather in terms of assignment and comparison to other theoretical or experimental results.

### B. Performance of the CVS-EOM-CCSD variants

Next we turn our attention to the performance of the different approximations that can be employed on top of CVS (see Section III A for their description). Our results for the  $X^-$  systems are shown in Figure 3. As we see similar trends for Xe, the corresponding figure is shown in the supplemental information (Figure S1), along with results for the REW approach for the Cl— to  $I^-$  (Figures S2, S3 and S4) and HCl to HI (Figures S5, S6 and S7).

A first observation is that freezing the core orbitals in the ground-state CCSD calculation results in a significant lowering of the core ionization energies. This lowering is considerable if the frozen core is taken to represent all subvalence spinors (FC-V), and it remains non-negligible even if the same threshold is used to define both the frozen orbitals and the core-valence separation region (FC-f). However, if one does not freeze the aimed edge (FC-fpMO), the ionization energy obtained is much closer to the corresponding CVS one.

Freezing all subvalence spinors but the ones in the edge we are interested in (FC-V-ex), an approximation that could provide potentially lower computational cost for systems with large number of core electrons such as the elements in the fourth row and beyond, does not perform better than (FC-f)—in fact, the opposite appears to be the case for the inner core orbitals.

Second, projecting out doubly-excited core excited determinants (ND) tends to result in an increase of the core ionization energies, which can be significant though always smaller than the underestimation produced by freezing all the core spinors.

As a result, the combination of these two approximations yields an approximate scheme that much better reproduces the CVS energies, though still with non-negligible discrepancies for the heavier elements. Particularly good results are shown by the (FC-ND-f) combination, for which error compensation yields results very similar to the regular CVS approximation. This can be rationalized because core correlation is not taken into account when using (FC-f), whereas the inclusion of the double occupied core orbitals in the EOM step does. Therefore, the combination of both approximations is in fact more consistent.

Since by using projection operators we do not save in memory or operation counts, the approximations discussed above are not of strong interest by themselves, and will not be used further since, even in the best combination, they will invariably degrade the performance of the original CVS scheme.

Therefore, combining the elimination of doubly core excited determinants with the use of a frozen core seems to yield a computationally efficient approach with a good error cancellation balance. In the case of heavy elements, if an efficient scheme for combining CVS and frozen core is to be implemented,<sup>15</sup> it may be interesting to keep a large frozen core (that would translate in potentially

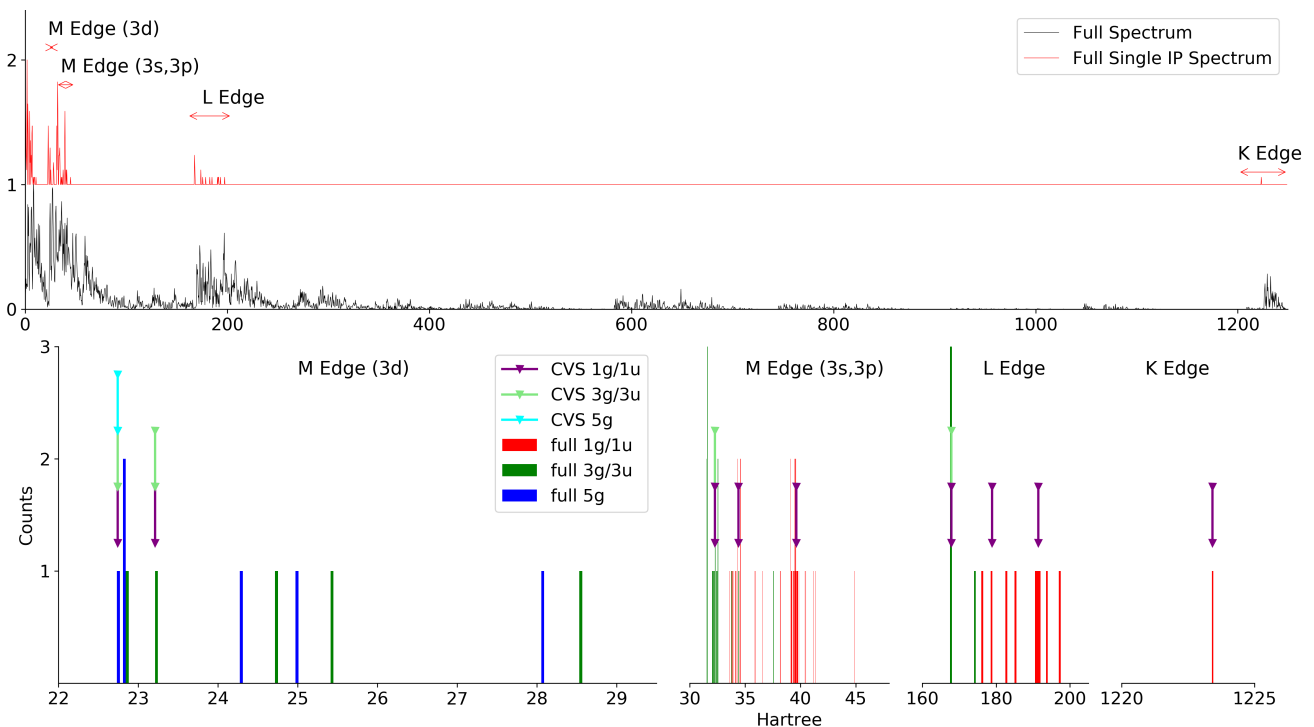


FIG. 2: Core ionization energies of iodide ( $\text{I}^-$ ) from full diagonalization of  $\bar{H}$ . Top: Representation of the eigenspectrum up to 1250 Ha, separated between all states (black) and those with non-negligible singly ionized contributions (red). Values in ordinate correspond to the number of states within a 0.37 Ha interval, with the largest value re-scaled to one. Bottom: Singly ionized states obtained by full diagonalization of  $\bar{H}$  and by the CVS approach. Intervals are 0.05, 0.5 and 0.037 Ha for the K, L and M edges, respectively. The labels  $ng/nu$  indicate the absolute value for the projection of the angular momentum ( $|m_j| = n/2, n = 1, 3, 5$ ), for the components of spinors of gerade (g) or ungerade (u) symmetry.

large computational savings), since combinations such as CVS-FC-ND-V seem to introduce non-negligible, but seemingly systematic, errors.

### C. Influence of the Hamiltonian on the core ionizations

Having established that CVS remains the most accurate approach compared to regular CCSD, we now turn our attention to the impact that the use of different Hamiltonians has on the ionization energies. Some of us have previously compared the DC and  ${}^2\text{DC}^M$  Hamiltonians, and established that they essentially provide the same results for valence excitation, ionization and electron attachment processes.<sup>27</sup> We can now extend such a comparison to core ionizations as well.

Our results can be found in Figure 4. First, we observe an extremely good match between the DC and  ${}^2\text{DC}^M$  Hamiltonians across the halogen series—that is, differences in absolute terms generally fall below 0.001 eV for the M edges, between around 0.01 and 0.1 eV for the L edges, and are of the order of 0.1 eV for the K edge of all species except astatine, for which the difference is 1.67 eV. This latter discrepancy, while not insignificant,

is still exceedingly small compared to the K edge binding energy of 96 keV.

This near-equality (in practical terms) means that any effects due to two-electron picture change effects are not very significant and, in our view, indicates that the 2-component molecular mean-field approach can be trusted for core properties, even for elements as heavy as those in the sixth row (and possibly including the actinides, though probably not for the superheavies and beyond). This is particularly important since 2-component approaches are intrinsically computationally more efficient in the AO transformation step, as they do not require the explicit consideration of small-component basis sets in the transformation.

Having established that the  ${}^2\text{DC}^M$  Hamiltonian can be safely used as an alternative to DC, we now compare it with the  ${}^2\text{DCG}^M$  and X2C Hamiltonians, which both incorporate spin-other orbit interactions. From these results, also shown in Figure 4, we clearly see that already starting with chloride, we have a non-negligible effect arising from the Gaunt interaction in  ${}^2\text{DCG}^M$  that lowers the core binding energy, and can amount to nearly 2 eV for the K edge.

For light elements, X2C and  ${}^2\text{DCG}^M$  are still quite

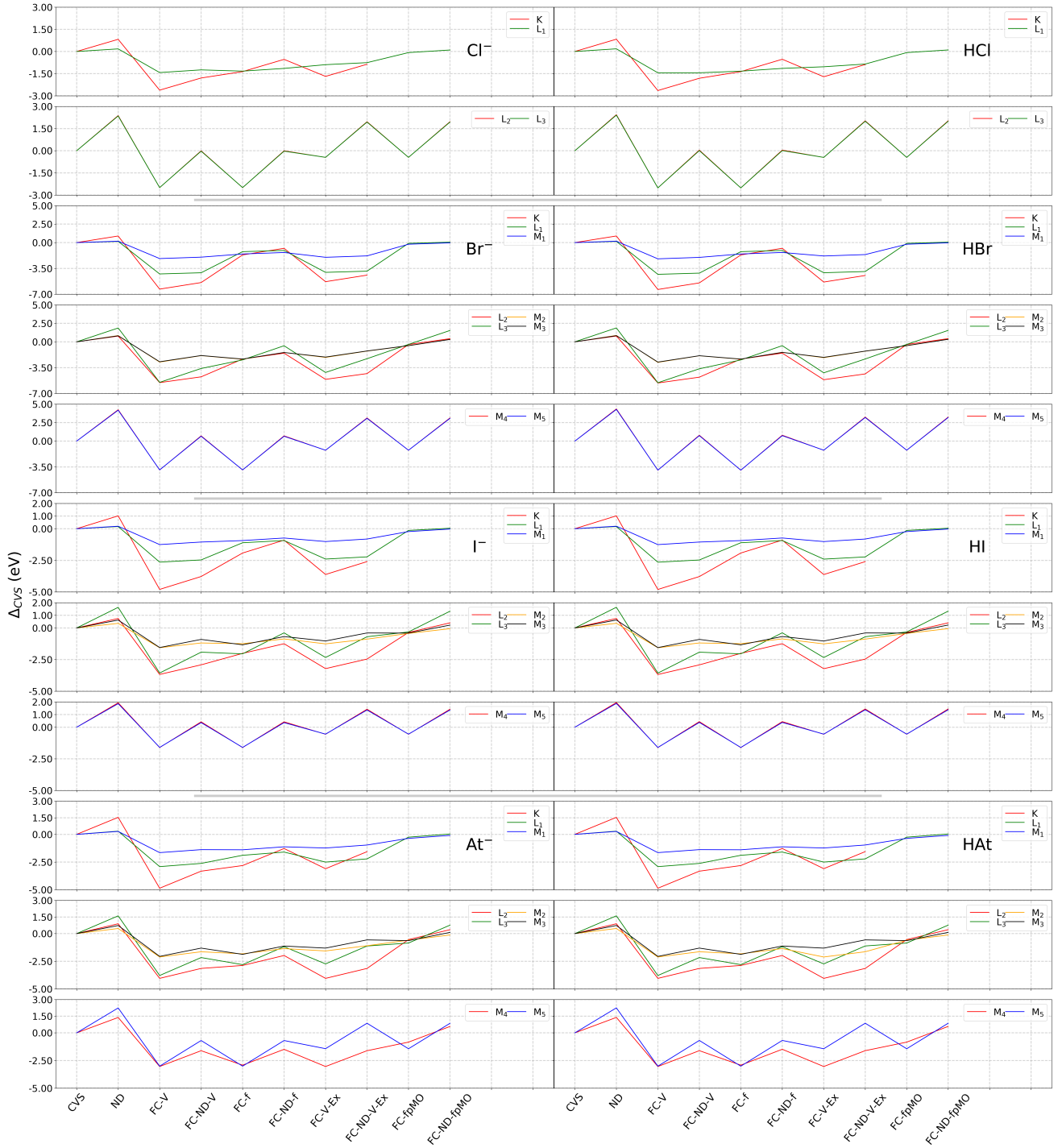


FIG. 3: Effect of the CVS variants on the binding energies of  $X^-$  and  $HX$  systems ( $X = \text{Cl}, \text{Br}, \text{I}$  and  $\text{At}$ ). Values (in eV) are relative to the original CVS approach.

close to each other, but as we progress down the rows of the periodic table, we see a rapidly increasing difference between the two, with significant differences not only for the K edge (with differences of over 40 eV for Iodine and

Xenon, and over 200 eV for Astatine) but for the L and M edges as well.

Finally, we assess the effect of including the  $(SS|SS)$  integrals in the 2-component based calculations ( $^2\text{DC}^M$

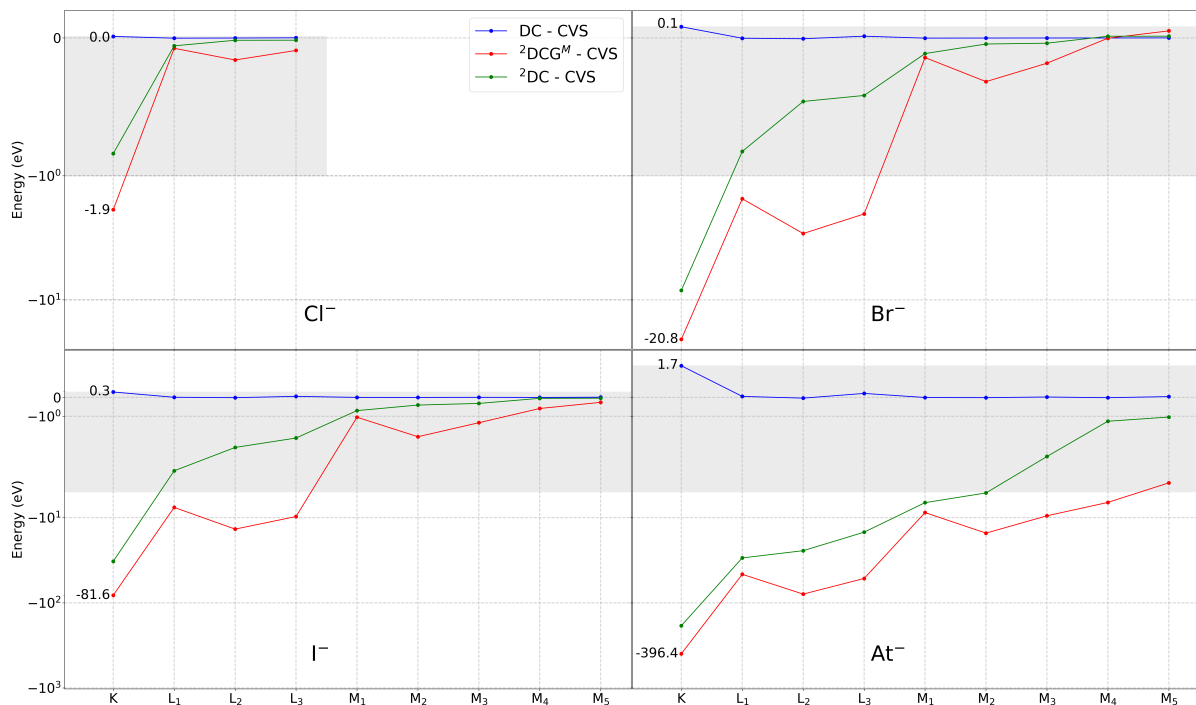


FIG. 4: Effects of the Hamiltonian on the binding energies (in eV) at different edges. The scales are logarithmic except for the areas in grey for which the scales are linear.

and  ${}^2\text{DCG}^M$ ). Since these contributions are generally very small for elements before the fourth row, and they increase significantly the cost of the SCF step, we have only investigated the fourth and fifth row atoms (I, Xe and At).

For  $\text{I}^-$  and Xe, these contributions are relatively modest, with reductions of around 2.6 eV and 3 eV, for the respective K edge binding energies. For the L edge binding energies, we observe reductions of around 0.4-0.7 eV, with the largest values being those for the  $\text{L}_2$  edges. For the  $\text{M}_1$  and  $\text{M}_2$  edges there are still reductions of around 0.1 eV, while for the remaining binding energies the effects tend to be around 0.01 eV.

We note that there is little variation from these atomic values for the molecular systems, in line with the much more localized nature of the small component density compared to the large component one. Furthermore, we notice a very subtle difference (0.02 eV) between the  ${}^2\text{DC}^M$  and  ${}^2\text{DCG}^M$  Hamiltonians with  $(SS|SS)$  integrals.

For  $\text{At}^-$  the reductions in binding energies are much more significant: for example, one has around 40 eV for the K edge and 10 eV for the  $\text{L}_2$  edge 7 eV, and values well above 1 eV for the  $\text{L}_3$  to  $\text{M}_2$  edges. Interestingly, these contributions remain around 0.5 eV for the N edges relating to ionizations from  $s$  and  $p$  spinors, which are comparable to the energies of the  $\text{M}_1$  and  $\text{M}_2$  edges for  $\text{I}^-$  and Xe, which fall between 0.7 and 1 keV.

Our results underline the need for explicitly accounting for these integrals (or correcting the energies for their

contribution), as soon as we are interested in edges arising from ionizations of  $s$  and  $p$  spinors for fifth-row elements and beyond. In the case one wants to explicitly account for them in correlated calculations, it is clear that the 2-component molecular mean field scheme would be the method of choice, given the substantial computational savings brought about by avoiding such integrals in the AO to MO transformation step.

#### D. Binding energies: comparison to experiment and prior theoretical works

We now compare our results, including the  $(SS|SS)$  integrals, to experiment and other theoretical results for the K and L edges of Xe,  $\text{XeF}_2$  and  $\text{CH}_3\text{I}$ , for which recent high energy, gas-phase XPS experiments have been performed (for Xe and  $\text{XeF}_2$ , results are also available for less energetic edges). Before doing so it should be recalled that all our calculations lack contributions from QED effects, and that the  ${}^2\text{DCG}^M$  does not include the gauge term that is necessary to recover the full (zero-frequency) Breit interaction.

Since we cannot, at this point, determine the QED and Breit contributions using DIRAC, we will combine our results with literature ones, such as those from Koziol and Aucar,<sup>48</sup> who provide the values for the Breit and leading QED contributions (self interaction and vacuum polarization) to the atomic spinors of selected closed-shell atoms (among which Xe) to determine energy correc-



TABLE I: Contributions (in eV) to the core binding energies of  $\text{I}^-$ ,  $\text{Xe}$  and  $\text{At}^-$  from: (a) the Gaunt interaction and (b) the  $(SS|SS)$  integral. These contributions are calculated as energy difference between CVS-EOM-CCSD calculations employing (a) the  $^2\text{DCG}^M$  and  $^2\text{DC}^M$  Hamiltonians; and (b) the  $^2\text{DCG}^M$  without and with inclusion of the  $(SS|SS)$  integrals at the SCF step.

Edge	$\text{I}^-$		$\text{Xe}$		$\text{At}^-$	
	$\Delta E(a)$	$\Delta E(b)$	$\Delta E(a)$	$\Delta E(b)$	$\Delta E(a)$	$\Delta E(b)$
K	-81.57	-2.58	-86.75	-2.87	-396.04	-40.50
L <sub>1</sub>	-7.59	-0.39	-8.15	-0.44	-46.24	-7.28
L <sub>2</sub>	-13.64	-0.58	-14.62	-0.65	-78.99	-10.46
L <sub>3</sub>	-9.70	-0.21	-10.39	-0.23	-51.77	-3.56
M <sub>1</sub>	-1.05	-0.08	-1.14	-0.09	-8.72	-1.79
M <sub>2</sub>	-2.08	-0.21	-2.25	-0.12	-15.19	-2.35
M <sub>3</sub>	-1.34	-0.08	-1.46	-0.04	-9.51	-0.89
M <sub>4</sub>	-0.59	-0.06	-0.66	-0.03	-6.62	-0.82
M <sub>5</sub>	-0.26	-0.04	-0.31	0.01	-4.52	-0.09
N <sub>1</sub>					-1.81	-0.44
N <sub>2</sub>					-3.29	-0.55
N <sub>3</sub>					-1.81	-0.19
N <sub>4</sub>					-0.91	-0.10
N <sub>5</sub>					-0.42	0.02
N <sub>6</sub>					6.74	0.06
N <sub>7</sub>					0.48	0.12

tions to our results. These results have been used by Southworth *et al.*<sup>49</sup> to correct their calculations, which are based on a combination of 1-component CVS-EOM-CCSD (and CCSDT) calculations with energy estimates for the different effects (1- and 2-electron scalar relativity, spin-orbit coupling, nuclear size effects).

Taking the Xe atom, the QED effects are most important for the K and L<sub>1</sub> edges, lowering the associated binding energies by 42.7 and 5.5 eV, respectively. They are also non-negligible for the L<sub>3</sub> and M<sub>1</sub> edges, which are lowered respectively by 0.5 and 1.1 eV. The Breit interaction also lowers the binding energies and, apart from the L<sub>1</sub> edge, for which both are of the same magnitude, is in general much larger than the QED effects (80.7, 13.1 and 8.8 eV for the K, L<sub>2</sub> and L<sub>3</sub> edges, respectively) and still important for the M<sub>3</sub> edge (1.2 eV).

Since Koziol and Aucar only provide the full Breit term, we have estimated the magnitude of the gauge correction from the difference between our  $^2\text{DCG}^M$  results and their Breit values. From that, we have that the gauge term increases the binding energies by 6.04 eV for the K edge, 0.51 eV for the L<sub>1</sub> edge, and around 1.57 and 1.58 eV for the L<sub>2</sub> and L<sub>3</sub> edges, respectively.

Adding the QED and Breit corrections to our  $^2\text{DC}^M$  results and the QED and gauge corrections to our  $^2\text{DCG}^M$  results, we obtain 34567.22 eV for the Xe K edge, which amounts to a difference of +2.09 eV to experiment. If we employ the estimate for higher-order correlation contributions to EOM-CCSD from Southworth *et al.*,<sup>49</sup> which decreases the binding energies by 3.8 eV, the difference to experiment is now of -1.71 eV. This

value is in line with the one obtained by Southworth and coworkers (-1.42 eV).

TABLE II: Comparison between calculated and experimental gas-phase binding energies (in eV) for Xe,  $\text{XeF}_2$  and  $\text{CH}_3\text{I}$ . The calculated binding energies are broken down into the value obtained with (a) Koopmans theorem, (b) CVS-EOM-CCSD method; (c) CVS-EOM-CCSD with atomic corrections for QED and Breit (in the case of  $^2\text{DCG}^M$  results, corrections for the gauge term) interactions; and (d) higher-order correlation corrections by Southworth and coworkers on (c). Our results for the  $^2\text{DC}^M$  or  $^2\text{DCG}^M$  Hamiltonians include contributions from the  $(SS|SS)$  integrals. A: ANO-RCC basis set, D: Dyal basis set

Edge model		E(a)	E(b)	E(c)	E(d)
<b>Xe</b>					
K	D/ $^2\text{DC}^M$	34755.91	34690.60	34567.22	34563.42
	D/ $^2\text{DCG}^M$	34669.08	34603.85	34567.22	34563.42
	A/ $^2\text{DC}^M$	34755.89	34690.63	34567.24	34563.44
	A/ref. 50	34752.00	34690.90	34567.51	34563.71
	exp. 50				34565.13
L <sub>1</sub>	D/ $^2\text{DC}^M$	5509.35	5473.66	5460.49	
	D/ $^2\text{DCG}^M$	5501.17	5465.51	5460.49	
	exp. 51				5452.7
L <sub>2</sub>	D/ $^2\text{DC}^M$	5161.45	5122.38	5109.30	
	D/ $^2\text{DCG}^M$	5146.77	5107.77	5109.30	
	exp. 51				5106.7
L <sub>3</sub>	D/ $^2\text{DC}^M$	4835.59	4796.85	4787.51	
	D/ $^2\text{DCG}^M$	4825.15	4786.46	4784.51	
	exp. 51				4786.7
M <sub>4</sub>	D/ $^2\text{DC}^M$	708.13	689.63	689.01	688.31
	D/ $^2\text{DCG}^M$	707.46	688.98	689.01	688.31
	A/ref. 50	707.5	689.6	688.98	688.28
M <sub>5</sub>	exp. 50				689.23
	D/ $^2\text{DC}^M$	694.90	676.71	676.32	675.62
	D/ $^2\text{DCG}^M$	694.58	676.30	676.32	675.62
	A/ref. 50	694.6	676.7	676.08	675.38
	exp. 50				676.44
<b>XeF<sub>2</sub></b>					
K	D/ $^2\text{DC}^M$	34759.79	34693.30	34569.90	34566.00
	A/ $^2\text{DC}^M$	34759.76	34694.28	34570.89	34566.99
	A/ref. 50	34755.80	34694.50	34571.10	34567.20
	exp. 50				34567.4
M <sub>4</sub>	D/ $^2\text{DC}^M$	711.99	693.23	687.00	686.00
	A/ $^2\text{DC}^M$	711.74	693.11	686.87	685.87
	A/ref. 50	711.9	693.9	687.7	686.7
	exp. 52				692.09
M <sub>5</sub>	D/ $^2\text{DC}^M$	698.49	679.95	675.69	674.69
	A/ $^2\text{DC}^M$	698.46	680.03	675.78	674.78
	A/ref. 50	698.6	680.6	674.4	673.4
	exp.				679.31
<b>CH<sub>3</sub>I</b>					
K	D/ $^2\text{DCG}^M$	33278.46	33213.79	33180.89	
	exp. 53				33175.20
L <sub>1</sub>	D/ $^2\text{DCG}^M$	5244.04	5208.55	5203.95	
	exp. 53				5197.47

As the latter have employed the uncontracted ANO-

RCC basis, which is smaller in size by a few primitives, and contains less tight  $s$  and  $p$  functions than the basis set employed here, we decided to investigate the impact of changing the basis set to ANO-RCC. To do so, we performed calculations with the  ${}^2\text{DC}^M$  Hamiltonian, subsequently employing the aforementioned QED and Breit corrections. From these results we obtain differences with respect to experiment of -1.69 eV, which is consistent with our results using the Dyall basis sets.

We attribute the difference, of around -0.27 eV, to the non-additivity of relativistic and correlation effects. That is perhaps better highlighted by the breakdown into mean-field and post mean-field (EOM-CCSD) contributions in the two cases: Southworth and coworkers' mean-field contributions to the binding energy are 3.89 eV smaller than ours, whereas their post-mean field correlations are 4.16 eV larger than ours, but since these have opposite signs the differences largely cancel. This points to the need to carefully benchmark additive approaches for elements beyond the fifth row, since for them the balance between electron correlation and relativistic effects is not necessarily the same as for the lighter elements.<sup>54</sup>

Beyond the K edge, after inclusion of the QED + Breit/Gauge corrections, we obtain 5466.02 eV, 5109.34 eV and 4788.04 eV for the binding energies of the  $L_1$ ,  $L_2$  and  $L_3$  edges, respectively. Compared to the results of *Oura et al.*<sup>51</sup> (5452.7 eV, 5106.7 eV and 4786.7 eV; measurements carried out at BL29XU of SPring-8 in May 2016), we note that our  $L_2$  edge shows slightly higher differences to experiment (2.6 eV) than the K edge, whereas for our  $L_3$  edges the difference is slightly lower (0.81 eV). For the  $L_1$  edge, on the other hand, we show the largest discrepancy to experiment (7.79 eV).

For the M edges, *Southworth et al.*<sup>50</sup> present experimental results for the  $M_{4,5}$  edges, and at 688.31 eV and 675.62 eV, our calculations (including the QED and Breit corrections as well as the higher-order correlation corrections from Southworth and coworkers<sup>50</sup>) differ from experiment by -0.94 eV and -0.85 eV respectively. For the  $M_4$  edge these are quite comparable to the theoretical calculations of Southworth and coworkers,<sup>50</sup> now corrected for QED effects (-0.92 eV to experiment), while for the  $M_5$  edge both theoretical results differ by around 0.24 eV.

Given the values for the higher-order correlation effects for the K and  $M_{4,5}$  edges, and from the breakdown of relativistic, correlation and QED effects from atomic many-body calculations on Xe at the K, L and M edges<sup>55</sup>—which indicate non-negligible differential correlation, relaxation and other effects (for example Auger shifts) for the different L edges, and to a lesser extent for the M edges—it becomes of great interest to attempt to investigate higher-order electron correlation corrections for the L edges.

For  $\text{XeF}_2$ , applying the same corrections as above to our  ${}^2\text{DC}^M$  and  ${}^2\text{DCG}^M$  calculations in the Dyall basis sets, we arrive at K edge binding energies of 34566.97 eV and 34566.99 eV respectively, which places our results

at -0.43 eV and -0.45 eV from experiment. These differences are smaller but still fairly consistent with those obtained for Xe, and together with the roughly constant shift of around 3.3–3.7 eV, irrespective of the Hamiltonian employed between the molecular and atomic values, emphasize the largely atomic nature of these deep core energies.

The breakdown of the energy contributions by *Southworth et al.* also points to the similarity between the core states of  $\text{XeF}_2$  and Xe. However, their results are closer to experiment for the molecule (-0.2 eV) than ours. To investigate this point, we have also performed  ${}^2\text{DC}^M$  calculations with the ANO-RCC basis, and after correcting these for Breit, QED and electron correlation, we obtain values which are consistent with our calculations employing the Dyall basis sets (-0.41 eV from experiment), which, once more, stresses the non-additivity of electron correlation and relativistic effects.

For the  $M_{4,5}$  edges, at EOM-CCSD level our results show differences to experiment of about 0.7 and 1 eV, respectively. These are quite close to the EOM-CCSD values of *Southworth et al.*,<sup>50</sup> and upon including the triples corrections from *Southworth et al.* (-1 eV), the calculated values shown an extremely good agreement with experiment. That is however fortuitous since, after correcting for QED and Breit interactions, our calculated values underestimate experiment by roughly 6.4 eV for the  $M_4$  edge, and 4.8 eV for the  $M_5$  edge.

For  $\text{CH}_3\text{I}$ , we have only performed  ${}^2\text{DCG}^M$  calculations, first because there are no significant differences between  ${}^2\text{DCG}^M$  and  ${}^2\text{DC}^M$  based results once we account for QED and Breit or gauge contributions, as the calculations for Xe and  $\text{XeF}_2$  illustrate. Second, in the  $C_s$  point group used, the coupled-cluster wavefunctions are complex-valued, making calculations computationally more expensive. We obtain 33213.79 eV and 5208.55 eV for the K and  $L_1$  edge binding energies, values that overestimate the experimental values by 38.59 eV and 11.08 eV. For the K edge, this difference is rather close to the one found for the Xe and  $\text{XeF}_2$  species.

As we do not have the QED and Breit/gauge corrections by *Kozioł and Aucar*<sup>48</sup>, we have used instead corrections provided by *Boudjemia et al.*,<sup>53</sup> which amount, for the K edge, to -77.0 eV for Breit, +6.10 eV for the gauge term and -39.0 eV for QED, and to -7.20 eV, +0.50 eV and -5.10 eV for the  $L_1$  edge. With these corrections, we now overestimate the K and  $L_1$  binding energies by 5.69 eV and 1.95 eV. The missing effect would be that of higher-order correlation corrections. While we cannot estimate this here, we speculate that if it follows roughly what is found for the Xe species, that would decrease the binding energies, and likely take the K edge to a few eV.

### E. Excitation energies: comparisons to experiment and prior theoretical works

As anticipated, the current implementation allows calculation not only of ionization energies, but also of excitation energies, which will be briefly discussed hereafter. In this case, since  $(SS|SS)$  integrals do not significantly affect the energies, only results for the  ${}^2\text{DCG}^M$  and  ${}^2\text{DC}^M$  Hamiltonian are presented, without explicit inclusion of the aforementioned integrals.

The results are shown in Table III, which displays selected excitation energies from different edges to the LUMO. We chose these particular transitions since both experimental and computational data are available in the literature,<sup>49,50</sup> which can be used as reference values. In particular, the experimental values are tabulated with the theoretical energies obtained in this study.

As already observed for the ionization processes, inclusion of the Gaunt interaction, accounting for the magnetic interaction between the electrons, lowers the excitation energy. This was expected as, in general, the inclusion of this term shifts the orbital energies of the inner core orbitals up (or lowers them, in term of absolute energy) and, at the same time, it reduces the spin-orbit coupling,<sup>20</sup> which is also reflected by the results reported herein. Indeed, the difference in the excitation energy from  $3d_{3/2}$  and  $3d_{5/2}$  to LUMO is slightly higher when the  ${}^2\text{DC}^M$  Hamiltonian is employed.

Upon inclusion of the Gaunt term in the Hamiltonian, the excitation energies differ by at most 0.4% from the corresponding experimental value, specifically for  $1s(\text{F})$ . This mismatch is higher than the others, which can be due to the fact that the CVS space was reduced so that this was the highest orbital, necessary in order to get this excitation. Thus, this space excludes the  $3d$  orbitals and in particular  $3d_{3/2}$ . The next higher disagreement between theory and experiment is found when exciting the  $1s(\text{Xe})$ , although by only 0.1%. Finally, the best agreement is found for both  $3d$  orbitals, with an error of only 0.04% ( $3d_{3/2}$ ) and 0.02% ( $3d_{5/2}$ ) from experiment. The computed energies are thus within the experimental error. In order to obtain the excitation from the  $(3d_{3/2})$  orbital, the same strategy of excluding all higher orbitals from the CVS space, hence excluding  $(3d_{5/2})$ , might be the reason of the subtly larger disagreement.

Nonetheless, these errors are actually quite small. Therefore, we can conclude that the CVS-EOM-CC method implemented in this work gives satisfactory core excitation energies.

## V. CONCLUSIONS

We have presented an implementation of the core-valence separation for the equation-of-motion coupled-cluster method in the DIRAC program. This implementation, which is based on a flexible framework for defining projection operators, enables the calculation ionization

TABLE III:  $\text{XeF}_2$ . Comparison between experimental gas-phase excitation energies and calculations (in eV). The calculated excitation energies have been obtained at the CVS-EOM-CCSD level of theory using the  ${}^2\text{DC}^M$  and the  ${}^2\text{DCG}^M$  Hamiltonians without contributions from the  $(SS|SS)$  integrals and the Dyall (D) basis set

Edge	transition	model	E
K	$1s(\text{Xe}) \rightarrow \text{LUMO}$	$\text{D}/{}^2\text{DC}^M$	34686.70
		$\text{D}/{}^2\text{DCG}^M$	34599.95
		exp. <sup>49</sup>	34557.4
	$1s(\text{F}) \rightarrow \text{LUMO}$	$\text{D}/{}^2\text{DC}^M$	685.91
		$\text{D}/{}^2\text{DCG}^M$	685.70
		exp. <sup>50</sup>	$682.8 \pm 0.3$
$\text{M}_4$	$3d_{3/2} \rightarrow \text{LUMO}$	$\text{D}/{}^2\text{DC}^M$	683.71
		$\text{D}/{}^2\text{DCG}^M$	683.06
		exp. <sup>50</sup>	$682.8 \pm 0.3$
$\text{M}_5$	$3d_{5/2} \rightarrow \text{LUMO}$	$\text{D}/{}^2\text{DC}^M$	670.34
		$\text{D}/{}^2\text{DCG}^M$	670.04
		exp. <sup>50</sup>	$669.9 \pm 0.3$

and excitation energies for all 4-component based Hamiltonians available in DIRAC, and consequently for non-relativistic Hamiltonians as well. We have applied our implementation to the calculation of core electron binding energies for halogen ( $\text{CH}_3\text{I}$ ,  $\text{X}^-$ , and  $\text{HX}$ ,  $\text{X} = \text{Cl}-\text{At}$ ) and Xe species ( $\text{Xe}$ ,  $\text{XeF}_2$ ). For the latter, we also briefly explored the calculation of core excitations. With these systems, we have investigated the performance of different approximations to the original CVS approach, the basis set effects, and the performance of different classes of 2-component approximations, based on atomic or molecular mean-field treatments of relativity.

For highly symmetric species such as the lighter halides, for which we are able to exactly diagonalize the original similarity-transformed Hamiltonian, we show that the CVS energies closely match those from exact diagonalization at all edges. For the overall test set, our assessment of the different approximations indicates the one which more closely matches the performance of the original CVS scheme employs both frozen core and the removal of doubly excited determinants containing only core occupied spinors. Taken individually, these approximations yield sizeable overestimations and underestimations to the core ionization energies, respectively.

With respect to the Hamiltonians, we observe first that molecular mean field 2-component calculations are nearly indistinguishable from the equivalent 4-component ones, though with numerical differences which are larger than those found in prior studies for valence properties. We see little different for the 2-component atomic and molecular mean field ones for low-energy ionizations (e.g. for the L edge for Cl, and L or M edges for Br, I or Xe), but from the K edge of the fourth row onwards, apart from a very significant difference (around 50 eV for iodine, for example), with the molecular mean field showing the best performance. Together with the fact that non-negligible contributions from the explicit consideration of

SSSS-type integrals start to be seen for the K edge of the fourth row, we consider the molecular mean field scheme to be preferred over the atomic mean field one.

A comparison to experimental results for Xe, XeF<sub>2</sub> and CH<sub>3</sub>I underscores the importance of the QED, Breit and higher order correlation effects to approach experimental results. While our calculations including the Gaunt interaction recover a significant fraction of the Breit interaction, the gauge term remains quite significant for the K and L edges, and it must be accounted for. For Xe, we have shown that, though our 4-component based CVS-EOM-CCSD approach and a more approximate one based on correcting 1-component CVS-EOM-CCSD calculations closely follow each other, non-negligible differences remain, that we attribute to the non-additivity of relativistic and electron correlation effects.

In view of these findings, we consider the 4-component based CVS-EOM-CCSD as a reliable approach for investigating core properties throughout the periodic table. Apart from its intrinsic interest, it may serve as a basis for further investigations of the reliability of more approximate schemes for atoms beyond the fifth row, as well as to verify whether such approximations result in significant changes for properties such as transition moments, that require the determination of the excited-state wavefunctions.

## VI. ACKNOWLEDGEMENTS

ASPG and LH acknowledge support from PIA ANR project CaPPA (ANR-11-LABX-0005-01), the Franco-German project CompRIXS (Agence nationale de la recherche ANR-19-CE29-0019, Deutsche Forschungsgemeinschaft JA 2329/6-1), I-SITE ULNE projects OVERSEE and MESONM International Associated Laboratory (LAI) (ANR-16-IDEX-0004), the French Ministry of Higher Education and Research, region Hauts de France council and European Regional Development Fund (ERDF) project CPER CLIMIBIO, and the French national supercomputing facilities (grants DARI A0050801859, A0070801859). MLV and SC acknowledge support from DTU Chemistry (start-up Ph.D. grant), and from the Independent Research Fund Denmark—Natural Sciences, Research Project 2, grant no. 7014-00258B. Support from the COST action CM1405 *MOLIM: Molecules in Motion* (short-term mobility grant to MLV to visit ASPG) is also acknowledged.

<sup>1</sup>J. Stöhr, *NEXAFS Spectroscopy*, Springer, Berlin, 1992.

<sup>2</sup>P. Norman and A. Dreuw, *Chem. Rev.*, 2018, **118**, 7208–7248.

<sup>3</sup>*X-Ray Absorption and X-ray Emission Spectroscopy; Theory and Applications*, ed. J. van Bokhoven and C. Lamberti, Wiley & Sons, 2016.

<sup>4</sup>*Synchrotron Radiation: Basics, Methods and Applications*, ed. S. Mobilio, F. Boscherini and C. Meneghini, Springer, 2014.

<sup>5</sup>*X-Ray Free Electron Lasers: Applications in Materials, Chemistry and Biology*, ed. U. Bergmann, V. Yachandra and J. Yano, Royal Society of Chemistry, 2017.

- <sup>6</sup>M. Nisoli, P. Decleva, F. Calegari, A. Palacios and F. Martín, *Chem. Rev.*, 2017, **117**, 10760–10825.
- <sup>7</sup>C. Milne, T. Penfold and M. Chergui, *Coord. Chem. Rev.*, 2014, **277–278**, 44–68.
- <sup>8</sup>C. South, A. Shee, D. Mukherjee, A. K. Wilson and T. Saue, *Phys. Chem. Chem. Phys.*, 2016, **18**, 21010–21023.
- <sup>9</sup>X. Zheng and L. Cheng, *J. Chem. Theory Comput.*, 2019, **15**, 4945–4955.
- <sup>10</sup>J. Stanton and R. Bartlett, *J. Chem. Phys.*, 1993, **98**, 7029–7039.
- <sup>11</sup>K. Sneskov and O. Christiansen, *WIREs Comput. Mol. Sci.*, 2012, **2**, 566–584.
- <sup>12</sup>L. S. Cederbaum, W. Domcke and J. Schirmer, *Phys. Rev. A: At. Mol. Opt. Phys.*, 1980, **22**, 206–222.
- <sup>13</sup>S. Coriani and H. Koch, *J. Chem. Phys.*, 2015, **143**, 181103.
- <sup>14</sup>S. Coriani and H. Koch, *J. Chem. Phys.*, 2016, **145**, 149901.
- <sup>15</sup>M. L. Vidal, X. Feng, E. Epifanovsky, A. I. Krylov and S. Coriani, *J. Chem. Theory Comput.*, 2019, **15**, 3117–3133.
- <sup>16</sup>B. N. C. Tenorio, T. Moitra, M. A. C. Nascimento, A. B. Rocha and S. Coriani, *J. Chem. Phys.*, 2019, **150**, 224104.
- <sup>17</sup>R. Faber and S. Coriani, *Phys. Chem. Chem. Phys.*, 2020, **22**, 2642.
- <sup>18</sup>K. Nanda, M. L. Vidal, R. Faber, S. Coriani and A. I. Krylov, *Phys. Chem. Chem. Phys.*, 2020, **22**, 2629.
- <sup>19</sup>K. G. Dyall and K. F. Jr., *Introduction to Relativistic Quantum Chemistry*, Oxford University Press, 2007.
- <sup>20</sup>T. Saue, *ChemPhysChem*, 2011, **12**, 3077.
- <sup>21</sup>J. P. Carbone, L. Cheng, R. H. Myhre, D. Matthews, H. Koch and S. Coriani, in *State of The Art of Molecular Electronic Structure Computations: Correlation Methods, Basis Sets and More*, ed. L. U. Ancarani and P. E. Hoggan, Academic Press, 2019, vol. 79 of *Advances in Quantum Chemistry*, pp. 241 – 261.
- <sup>22</sup>J. Liu, D. Matthews, S. Coriani and L. Cheng, *J. Chem. Theory Comput.*, 2019, **15**, 1642–1651.
- <sup>23</sup>M. L. Vidal, P. Pokhilko, A. I. Krylov and S. Coriani, *J. Phys. Chem. Lett.*, 2020, **11**, 8314–8321.
- <sup>24</sup>L. Keller, V. Blum, P. Rinke and D. Golze, *J. Chem. Phys.*, 2020, **153**, 114110.
- <sup>25</sup>C. Fillaux, C. Den Auwer, D. Guillaumont, D. K. Shuh and T. Tylliszczak, *J. Alloys Compd.*, 2007, **444–445**, 443–446.
- <sup>26</sup>P. S. Bagus, E. S. Ilton and C. J. Nelin, *Surf. Sci. Rep.*, 2013, **68**, 273–304.
- <sup>27</sup>A. Shee, T. Saue, L. Visscher and A. S. P. Gomes, *J. Chem. Phys.*, 2018, **149**, 174113.
- <sup>28</sup>T. Saue, R. Bast, A. S. P. Gomes, H. J. A. Jensen, L. Visscher, I. A. Aucar, R. Di Remigio, K. G. Dyall, E. Eliav, E. Fasshauer, T. Fleig, L. Halbert, E. D. Hedegård, B. Helmich-Paris, M. Iliaš, C. R. Jacob, S. Knecht, J. K. Laerdahl, M. L. Vidal, M. K. Nayak, M. Olejniczak, J. M. H. Olsen, M. Pernpointner, B. Senjean, A. Shee, A. Sunaga and J. N. P. van Stralen, *J. Chem. Phys.*, 2020, **152**, 204104.
- <sup>29</sup>A. I. Krylov, *Ann. Rev. Phys. Chem.*, 2008, **59**, 433–462.
- <sup>30</sup>A. Dreuw and M. Wormit, *WIREs Comput. Mol. Sci.*, 2015, **5**, 82–95.
- <sup>31</sup>L. Visscher, T. J. Lee and K. G. Dyall, *J. Chem. Phys.*, 1996, **105**, 8769–8776.
- <sup>32</sup>M. Pernpointner and L. Visscher, *J. Comp. Chem.*, 2003, **24**, 754–759.
- <sup>33</sup>A. Shee, L. Visscher and T. Saue, *J. Chem. Phys.*, 2016, **145**, 184107.
- <sup>34</sup>DIRAC, a relativistic ab initio electronic structure program, Release DIRAC19 (2019), written by A. S. P. Gomes, T. Saue, L. Visscher, H. J. A. Jensen, and R. Bast, with contributions from I. A. Aucar, V. Bakken, K. G. Dyall, S. Dubillard, U. Ekström, E. Eliav, T. Enevoldsen, E. Faßhauer, T. Fleig, O. Fossgaard, L. Halbert, E. D. Hedegård, B. Helmich-Paris, T. Helgaker, J. Henriksson, M. Iliaš, Ch. R. Jacob, S. Knecht, S. Komorovský, O. Kullie, J. K. Laerdahl, C. V. Larsen, Y. S. Lee, H. S. Nataraj, M. K. Nayak, P. Norman, G. Olejniczak, J. Olsen, J. M. H. Olsen, Y. C. Park, J. K. Pedersen, M. Pernpointner, R. di Remigio, K. Ruud, P. Salek, B. Schimmelpennig,



- B. Senjean, A. Shee, J. Sikkema, A. J. Thorvaldsen, J. Thyssen, J. van Stralen, M. L. Vidal, S. Villaume, O. Visser, T. Winther, and S. Yamamoto (available at <http://dx.doi.org/10.5281/zenodo.3572669>, see also <http://www.diracprogram.org>).
- <sup>35</sup>K. G. Dyall, *Theor. Chem. Acc.*, 2002, **108**, 335–340.
- <sup>36</sup>K. G. Dyall, *Theor. Chem. Acc.*, 2003, **109**, 284–284.
- <sup>37</sup>K. G. Dyall, *Theor. Chem. Acc.*, 2012, **131**, 1172.
- <sup>38</sup>K. G. Dyall, *Theor. Chem. Acc.*, 2016, **135**, 128.
- <sup>39</sup>R. A. Kendall, T. H. Dunning, Jr. and R. J. Harrison, *J. Chem. Phys.*, 1992, **96**, 6796.
- <sup>40</sup>J. Sikkema, L. Visscher, T. Saue and M. Iliaš, *J. Chem. Phys.*, 2009, **131**, 124116.
- <sup>41</sup>L. Visscher, *Theor. Chem. Acc.*, 1997, **98**, 68–70.
- <sup>42</sup>L. Cheng, J. Gauss and J. F. Stanton, *J. Chem. Phys.*, 2013, **139**, 054105.
- <sup>43</sup>*Structure of Free Polyatomic Molecules*, ed. K. Kuchitsu, Springer Berlin Heidelberg, 1998.
- <sup>44</sup>L. Visscher, J. Styszyński and W. C. Nieuwpoort, *J. Chem. Phys.*, 1996, **105**, 1987–1994.
- <sup>45</sup>L. Halbert, M. L. Vidal, A. Shee, S. Coriani and A. S. P. Gomes, *Dataset: Relativistic EOM-CCSD for core-excited and core-ionized state energies based on the 4-component Dirac-Coulomb(-Gaunt) Hamiltonian*, 2020, <https://doi.org/10.5281/zenodo.4118190>.
- <sup>46</sup>R. Sarangi, M. L. Vidal, S. Coriani and A. I. Krylov, *Mol. Phys.*, 2020, **0**, e1769872.
- <sup>47</sup>M. F. Herbst and T. Fransson, *J. Chem. Phys.*, 2020, **153**, 054114.
- <sup>48</sup>K. Koziol and G. A. Aucar, *J. Chem. Phys.*, 2018, **148**, 134101.
- <sup>49</sup>S. Southworth, R. Dunford, D. Ray, E. Kanter, G. Doumy, A. March, P. Ho, B. Krässig, Y. Gao, C. Lehmann *et al.*, *Phys. Rev. A*, 2019, **100**, 022507.
- <sup>50</sup>S. H. Southworth, R. Wehlitz, A. Picón, C. S. Lehmann, L. Cheng and J. F. Stanton, *J. Chem. Phys.*, 2015, **142**, 224302.
- <sup>51</sup>M. Oura, T. Gejo, K. Nagaya, Y. Kohmura, K. Tamasaku, M. N. Piancastelli and M. Simon, *New Journal of Physics*, 2019, **21**, 043015.
- <sup>52</sup>T. X. Carroll, R. W. Shaw Jr, T. D. Thomas, C. Kindle and N. Bartlett, *J. Am. Chem. Soc.*, 1974, **96**, 1989–1996.
- <sup>53</sup>N. Boudjemia, K. Jänkälä, T. Gejo, K. Nagaya, K. Tamasaku, M. Huttula, M. N. Piancastelli, M. Simon and M. Oura, *Phys. Chem. Chem. Phys.*, 2019, **21**, 5448–5454.
- <sup>54</sup>A. Gomes and L. Visscher, *Chem. Phys. Lett.*, 2004, **399**, 1–6.
- <sup>55</sup>T. Mooney, E. Lindroth, P. Indelicato, E. G. Kessler and R. D. Deslattes, *Phys. Rev. A*, 1992, **45**, 1531–1543.

**Supplemental Information: Relativistic EOM-CCSD for core-excited and core-ionized state energies based on the 4-component Dirac-Coulomb(-Gaunt) Hamiltonian.**

Loïc Halbert,<sup>1, a)</sup> Marta L. Vidal,<sup>2, b)</sup> Avijit Shee,<sup>3, c)</sup> Sonia Coriani,<sup>2, d)</sup> and André Severo Pereira Gomes<sup>1, e)</sup>

<sup>1)</sup> *Université de Lille, CNRS, UMR 8523 – PhLAM – Physique des Lasers, Atomes et Molécules, F-59000 Lille, France*

<sup>2)</sup> *Department of Chemistry, Technical University of Denmark, DK-2800 Kongens Lyngby, Denmark*

<sup>3)</sup> *Department of Chemistry, University of Michigan, Ann Arbor, Michigan 48109, USA*

The datasets, notebooks and figures are available at <https://doi.org/10.5281/zenodo.4116367>

---

<sup>a)</sup>Electronic mail: [loic.halbert@univ-lille.fr](mailto:loic.halbert@univ-lille.fr)

<sup>b)</sup>Electronic mail: [malop@kemi.dtu.dk](mailto:malop@kemi.dtu.dk)

<sup>c)</sup>Electronic mail: [ashee@umich.edu](mailto:ashee@umich.edu)

<sup>d)</sup>Electronic mail: [soco@kemi.dtu.dk](mailto:soco@kemi.dtu.dk)

<sup>e)</sup>Electronic mail: [andre.gomes@univ-lille.fr](mailto:andre.gomes@univ-lille.fr)

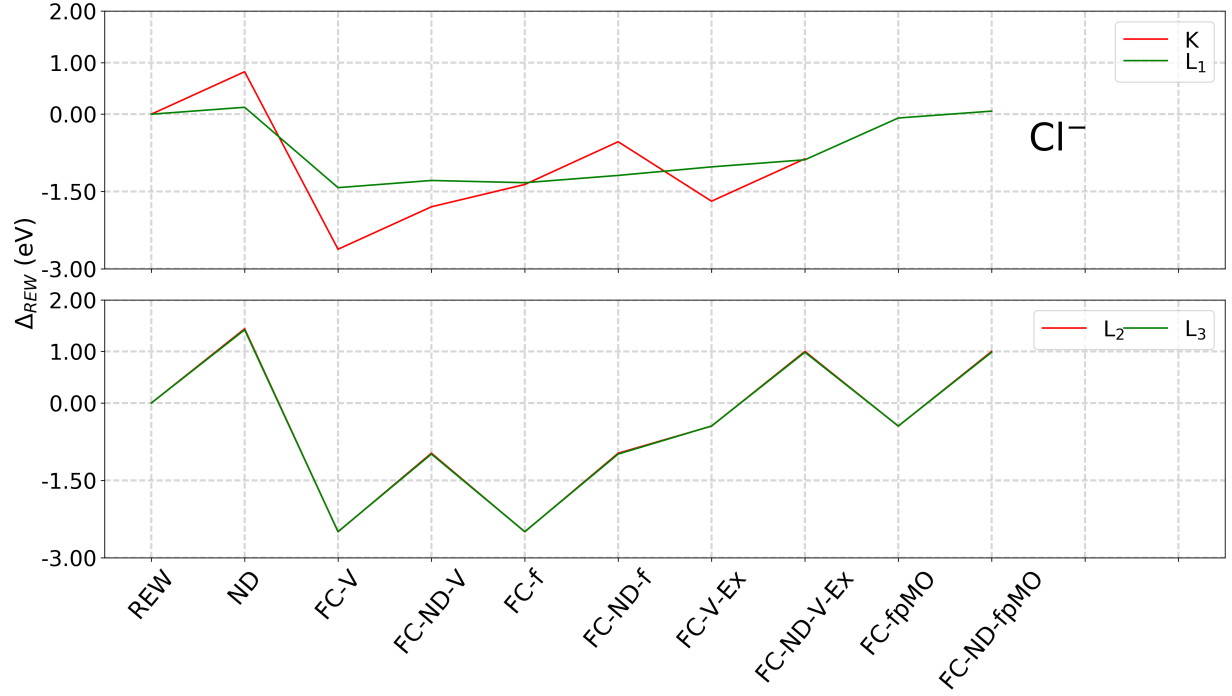


FIG. S2: Effect of the REW variants on the different binding energies of  $\text{Cl}^-$ . Values (in eV) are relative to the original REW approach.

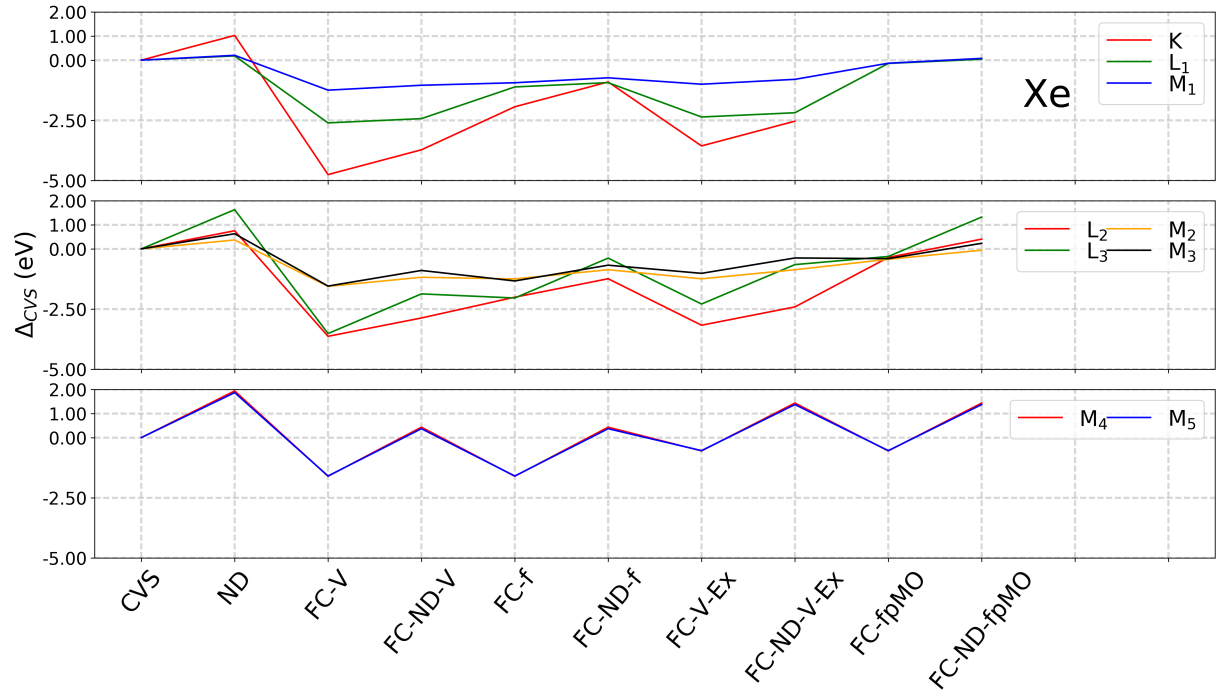


FIG. S1: Effect of the CVS variants on the different binding energies of Xe. Values (in eV) are relative to the original CVS approach.

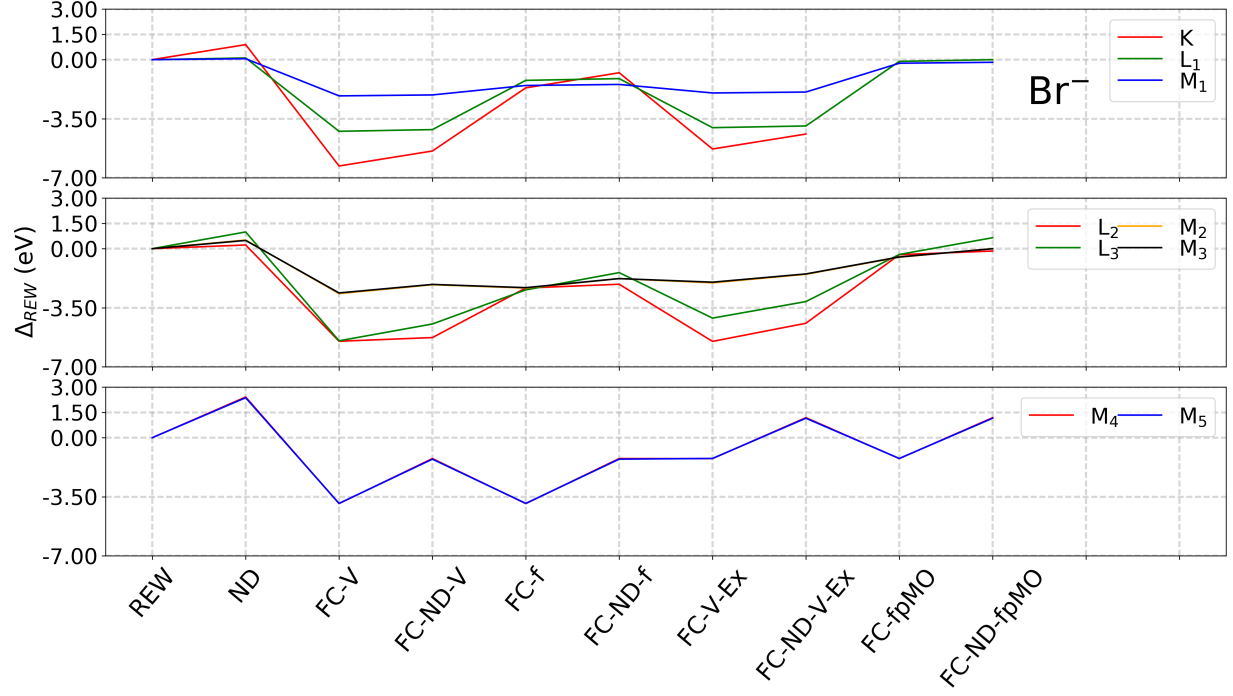


FIG. S3: Effect of the REW variants on the different binding energies of  $\text{Br}^-$ . Values (in eV) are relative to the original REW approach.

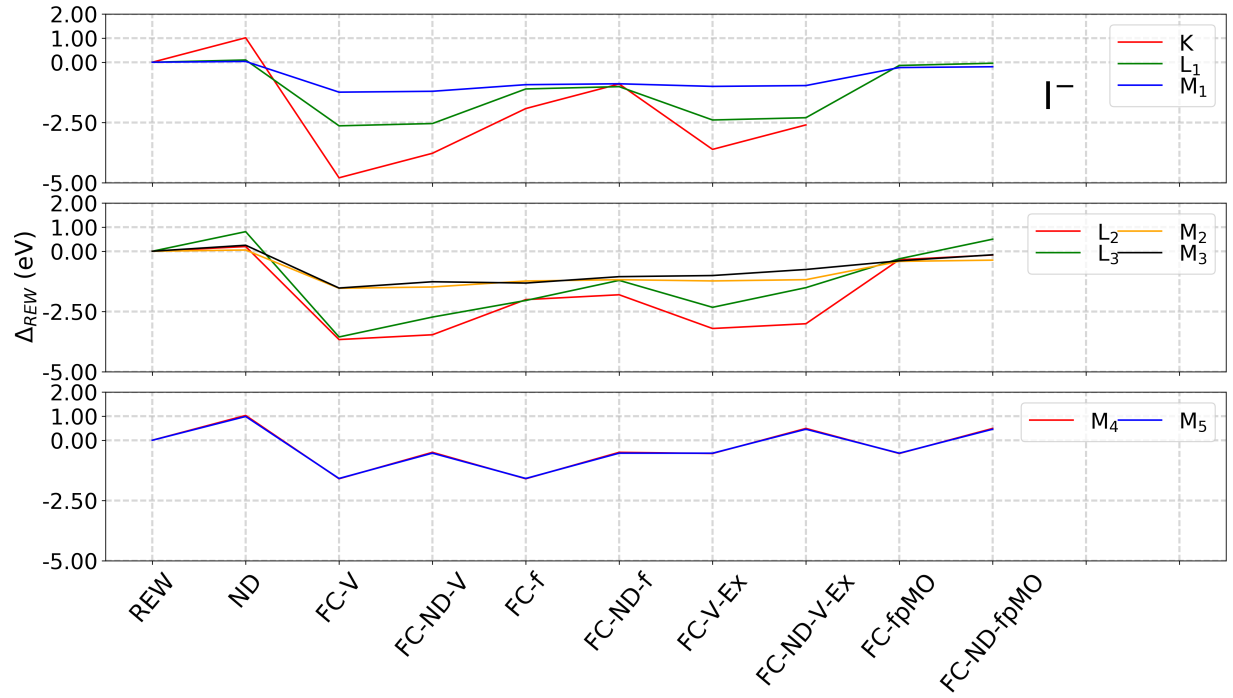


FIG. S4: Effect of the REW variants on the different binding energies of  $\text{I}^-$ . Values (in eV) are relative to the original REW approach.



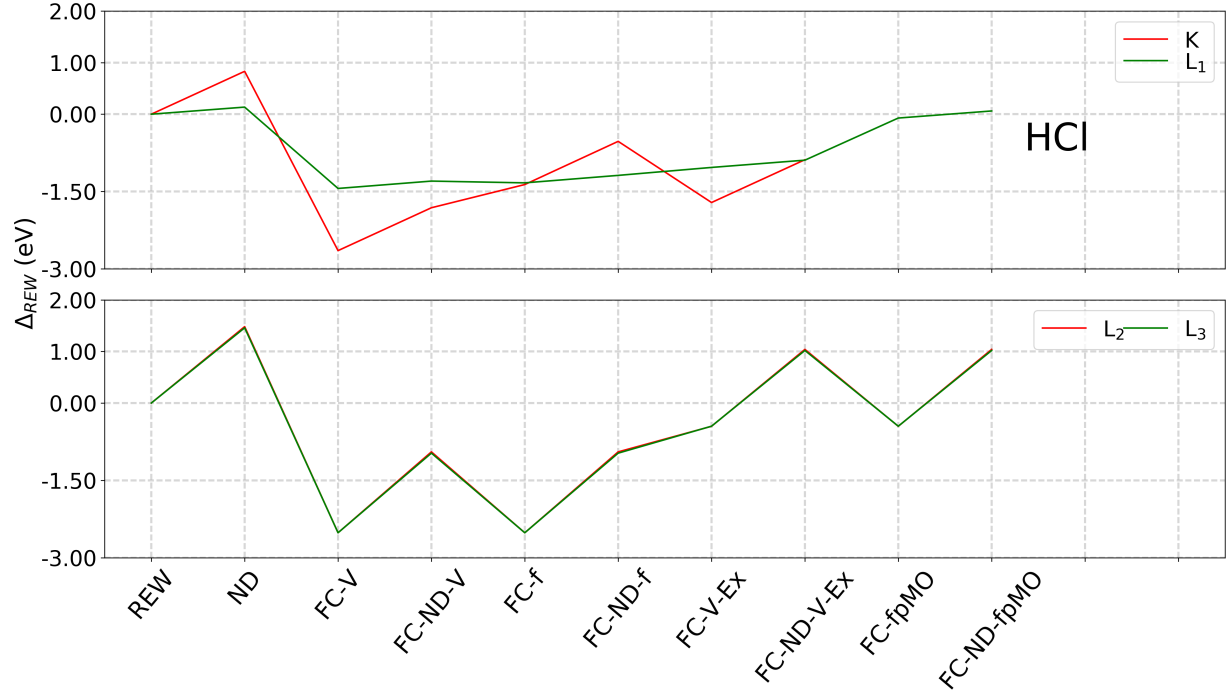


FIG. S5: Effect of the REW variants on the different binding energies of HCl. Values (in eV) are relative to the original REW approach.

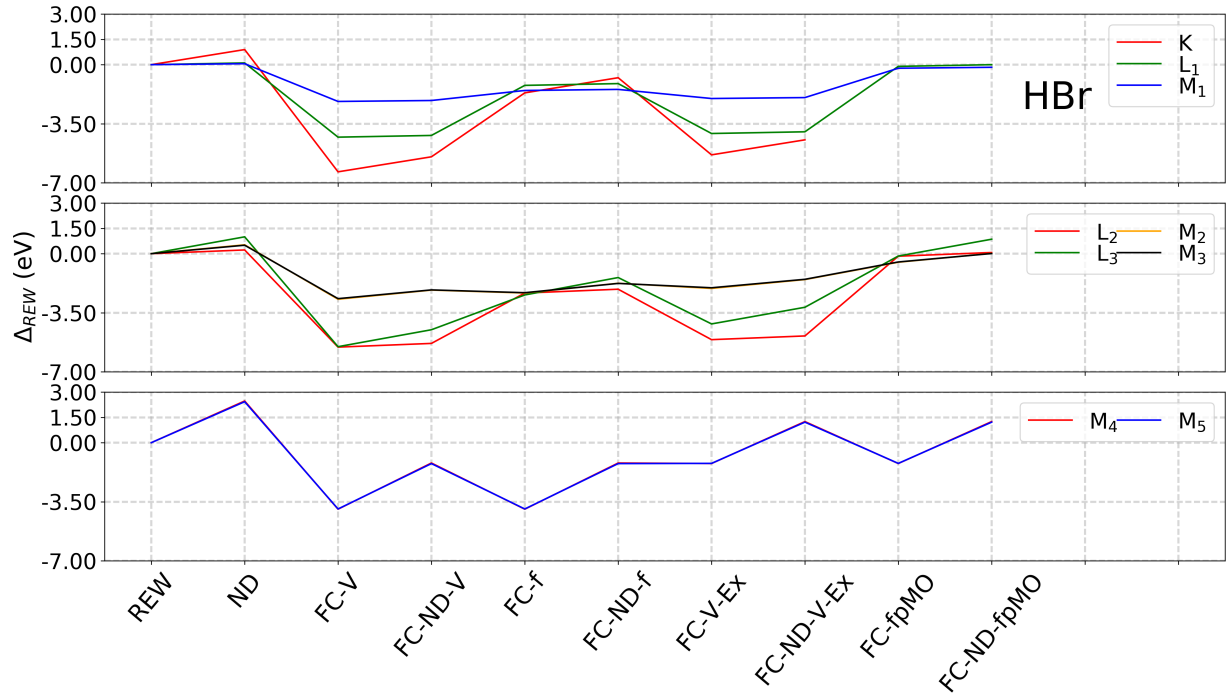


FIG. S6: Effect of the REW variants on the different binding energies of HBr. Values (in eV) are relative to the original REW approach.

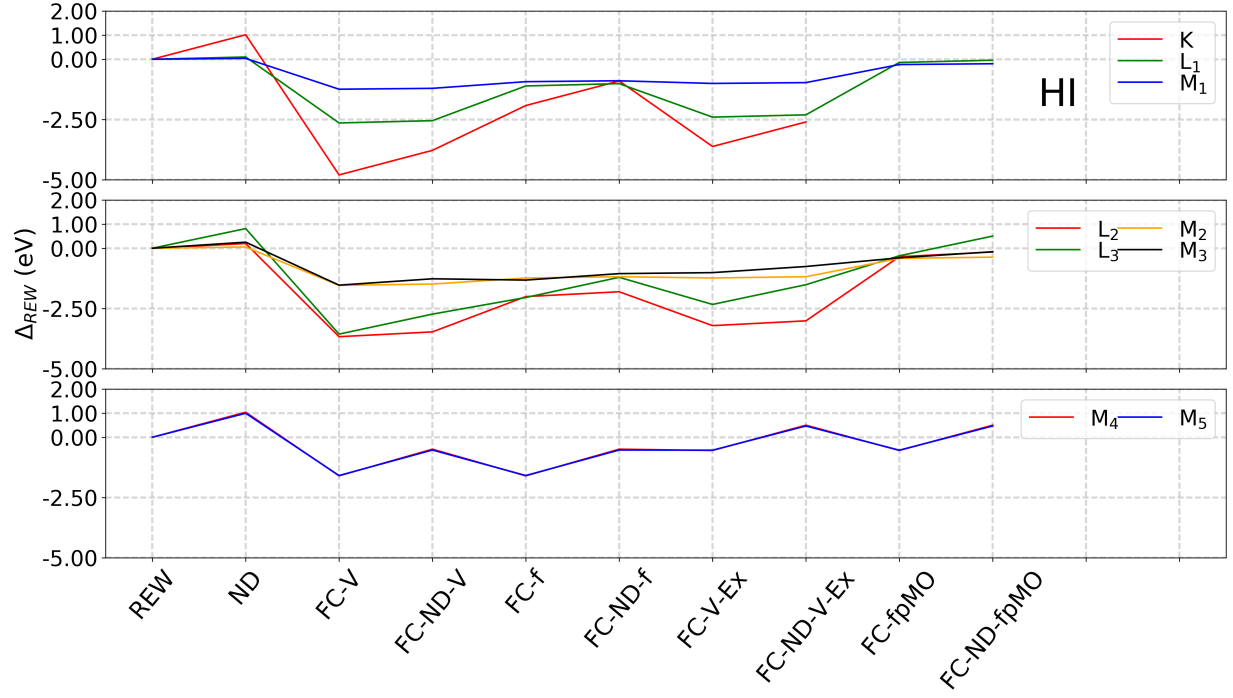


FIG. S7: Effect of the REW variants on the different binding energies of HI. Values (in eV) are relative to the original REW approach.